TARGET AND UNTARGETED GC-MS BASED METABOLOMIC STUDY OF MOUSE OPTIC NERVE AND ITS POTENTIAL IN THE STUDY OF NEUROLOGICAL VISUAL DISEASES

Carolina Gonzalez-Riano[1], Miriam Sanz-Rodríguez[2], Juan Escudero-Ramirez[2], M Paz. Lorenzo[1], Coral Barbas[1], Beatriz Cubelos[2], Antonia Garcia[1*]

[1]Centre for Metabolomics and Bioanalysis (CEMBIO), Facultad de Farmacia, Universidad CEU San Pablo, Campus Monteprincipe, Boadilla del Monte 28668, Madrid, Spain

[2] Departamento de Biología Molecular and Centro de Biología Molecular "Severo Ochoa", Universidad Autónoma de Madrid-Consejo Superior de Investigaciones Científicas, 28049, Madrid-Spain.

*Author to whom correspondence should be addressed

e-mail address: antogar@ceu.es

Center for Metabolomics and Bioanalysis (CEMBIO)

Faculty of Pharmacy

San Pablo CEU University

Campus Monteprincipe

Boadilla del Monte

28668 Madrid, Spain

Telephone number: 00 34 91 3724753

Fax: +34 913724712

Keywords: Metabolomics; Optic neuropathies; GC-MS; metabolomics; Method validation; Fingerprinting

Abbreviations:

NVD: Neurological Visual Disease

QEA: Quantitative enrichment analysis

GRAPHICAL ABSTRACT

ABSTRACT

The optic nerve is made of highly specialized neurons and the energetic supply to their axons is crucial due to their great demand. The energy comes basically through the oxidative phosphorylation in the mitochondria, supported by glial cells metabolism. Mitochondrial dysfunction is a shared feature encountered within the optic neuropathies, including Leber's Hereditary Optic Neuropathy, Leigh's Syndrome, or Kjer's syndrome.

In an effort to investigate the metabolic alterations produced within the optic nerve in a mutant mouse model of Neurological Visual Disease (NVD), a rapid, robust, and efficient one-single phase extraction methodology has been developed and validated for the GC-MS platform. Once the method was successfully validated for lactic acid and pyruvic acid as markers of an adequate optic nerve function, the protocol was applied to unveil the metabolomic signature of the wild-type mouse optic nerve. Along the chromatographic profile of the optic nerve, 94 peaks were identified and, to our knowledge, for the first time. Afterwards, a targeted metabolomics analysis was performed to quantify lactic acid and pyruvic acid in the NDV mice group (n = 8) and its corresponding wild-type (n = 8). Finally, an untargeted metabolomics study was carried out and univariate and multivariate data analyses showed 34 compounds modified in the optic nerve of the mouse with NVD mutation. Then, the metabolic reaction network of the identified metabolites highlighted alterations in the catabolism of proteins, TCA cycle, and urea cycle, reflecting a mitochondrial energetic dysfunction. Taken together, this metabolomics study has proven to be suited for the study of optic neuropathies.

1. INTRODUCTION

The nervous system includes a great variety of cell types (among others: astrocytes, neurons and oligodendrocytes), what makes one of the most complex tissues in the human body. The correct metabolic coupling between these cell types is key to allow the central nervous system (CNS) circuits' physiological performance. The optic nerve is the main myelinated neural tract in the CNS, a clear example of the importance of this mentioned metabolic coupling. When the normal flow of metabolites is altered, it can lead to several neurological pathologies such as Friederich Ataxia, Leber's Hereditary Optic Neuropathy, Leigh's Syndrome, Kjer's syndrome, etc. Among other symptoms, the common denominator of these pathologies is the alteration in the metabolic coupling in the optic nerve.

The identification of metabolomic biomarkers is an essential target for studying and understanding several neurological diseases. Nowadays, measurements of lactic acid and pyruvic acid levels are used as indicators of energetic metabolic defects in different neural circuits. Hence, they could be seen as key elements in order to study and comprehend metabolic-caused visual diseases.

Our laboratory counts on a mutant mouse which shows an altered metabolic coupling between the different CNS cell types. Therefore, this mutant mouse makes a powerful tool in order to study neurologic and metabolic diseases.

In this work, we present for the first time a metabolomics study in the optic nerve of Mice with Neurological Visual Disease (NVD) compared to wild-type animals.

Over the past decade, metabolomics, which attempts to detect, quantify and identify the widest possible range of metabolites integrating the metabolome of biological fluids, tissues, and cells, has proven to be a useful tool for several applications, including unveiling potential biomarkers for clinical diagnostics, studying the mechanism under different pathologies, pharmacological treatments, and environmental effects in different organisms, among others [1]. This is possible since the metabolites reflect the final products that different cellular and regulatory processes leave behind, providing a snap shot of the set of all these processes occurring at a specific moment. Despite the fact that a classification of different strategies for metabolomics studies was proposed [2, 3], the two mainly approaches employed in this field nowadays are the targeted and untargeted analysis. Targeted metabolomics is intended for the quantitative measurement of a predefined set of metabolites normally involved in a specific pathway or metabolic reaction. On the other hand, untargeted metabolomics scope is the analysis of as many metabolites as possible present in a biological system to identify novel pathophysiological pathways and uncover biomarkers [4]. The detection of all the mechanistic insights in a biological

sample has been greatly strengthened thanks to the remarkable improvement of the analytical platforms available and the development of new powerful bioinformatics tools [5, 6]. Analytical techniques based on mass spectrometry show extremely high potential in metabolomics and, in particular, the application of GC-MS platform provides high separation efficiency allowing the detection and quantification of metabolites involved into the central metabolic pathways, including amino acids, short and long chain free fatty acids, cholesterol, among others. All of them are low molecular weight compounds that can be converted into their volatile derivatives [7,8].

The optic nerve presents a great content of a wide variety of lipids classes, ranging between 50 to 60% of its dry weight, located in the myelinated and unmyelinated nerve areas, connective tissue, glial cells, and blood vessels [9, 10]. It also contains a high concentration of cytoskeletal proteins, considering neurofilaments, microtubules, microtubule associated proteins (MAPs), and actin as the principal constituents of the neuronal cytoskeleton, which confers a special hardness to the tissue [11]. Metabolomics studies of the optic nerve are scarce and mainly focused on the lipid composition [12, 13] and almost absent on the investigation of polar and small metabolites.

Based on the evidences previously described, GC- -MS was the configuration selected for the development and validation of a method for the absolute quantitation of lactic acid and pyruvic acid in optic nerve tissue samples of a mutant mice model and its corresponding control group (wild-type, WT), followed by an untargeted metabolomics approach and the characterization of the metabolic profile of the optic nerve.

2. MATERIALS AND METHODS

2.1. Samples

Mice were housed in specific pathogen-free conditions, humidity and temperature-controlled room on a 12-h light/dark cycle, receiving water and food ad libitum. All animal procedures were approved by the corresponding institutional ethical committee (CBMSO) and were performed in accordance with Spanish and European directives. All efforts were made to minimize animal suffering. Samples were obtained from four months WT and NVD mutant mice. After cervical dislocation, we proceeded with the immediate extraction and freezing of the optic nerves in liquid nitrogen.

2.2. Reagents

Lactic acid 98%, pyruvic acid 98%, pentadecanoic acid 99%, and methyl stearate standards 99% were purchased from Sigma-Aldrich (Steinheim, Germany). Reagents for derivatization (O-methoxyamine hydrochloride and BSTFA:TMCS, 99:1 (Sylon BFT)) were purchased from Sigma-

Aldrich (Steinheim, Germany) and Supelco (Bellefonte, PA, USA), respectively. Standard mix for GC-MS, containing grain fatty acid methyl esters (C8:0-C22:1, n9) and analytical grade heptane were purchased from Fluka Analytical (Sigma-Aldrich Chemie GmbH, Steinheim, Germany). Silylation-grade pyridine was from VWR International BHD Prolabo (Madrid, Spain). HPLC grade methanol was obtained as well from Sigma-Aldrich (Steinheim, Germany).

2.3. Sample treatment and GC-MS analysis

Sample preparation for GC-MS analysis was performed at CEMBIO (Madrid, Spain). Eight optic nerve samples from a mutant model (NVD) (n=4) and wild-type (WT) (n=4) mice, and 18 samples (NDV, *n*=8, and WT, *n*=8) were selected for validation of the method for target analysis of lactic acid and pyruvic acid and for non-targeted metabolomics studies respectively. All samples were stored at -80 ºC and the day of the analysis they were defrosted, followed by the addition of 100 µL of cold methanol (-20 ºC) containing the internal standard (IS) pentadecanoic acid (25 ppm). Then, samples were homogenized using a 2 mm particle size glass beads for the TissueLyser LT homogenizer (Qiagen, Germany), and placing samples on ice in between of TissueLyser cycles for 30 seconds, 6 times each. The extracted samples were then centrifuged at 13.000*g* at 4ºC for 10 min. For the validation of the method, all the supernatants (80 µL) were pooled, and then frozen at -80ºC, while for the metabolomics analysis, 80 µL of the supernatant of each sample was transferred into a GC-MS vial.

Afterwards, samples were chemically derivatized for GC-MS analysis. The 80 µL of supernatant previously collected were evaporated to dryness using a SpeedVac Concentrator System. Methoxymation was performed by adding 20 µL of *O*-methoxyamine hydrochloride (15 mg/mL in pyridine) to each sample and vigorously vortex-mixed for 5 min. Then, vials were incubated in darkness at room temperature for 16 hours. For silylation process, 20 µL of BSTFA:TMCS (99:1) were added, vortex-mixed for 5 min, and capped vials were placed in the oven at 70 ºC for 1 hour. Prior to injection, 100 µL of heptane containing C18:0 methyl ester (10 ppm) as instrumental IS was added and again vortex-mixed for 1 min to dissolve derivatives. Two blank solutions were prepared along with the rest of samples following the same procedure of extraction and derivatization and analyzed at the beginning and at the end of the sequence.

Quality control samples (QC) were prepared by pooling equal volumes (approx. 20 µL) of optic nerve homogenate from each of the 18 samples prior to the derivatization process. Four QC samples were independently prepared simultaneously with the study samples by dividing up the total volume of this pooled QC. In order to measure the performance and stability of the system together with the reproducibility of the sample treatment procedure, QC samples were analyzed every 6 samples throughout the run.

A flowchart of the method procedure for the GC-MS analysis of the optic nerve tissue samples is presented in Fig. 1.

FIGURE 1

2.4. Targeted and non-targeted Fingerprinting of Mouse Optic Nerve

Samples were prepared according to the previous extraction method and analyzed by GC-MS for targeted and non-targeted metabolomics analysis following the method described below. With the targeted approach, the absolute quantitation of lactic acid and pyruvic acid in optic nerve samples was performed by means of authentic analytical standards and with the non-targeted approach the metabolite profile was characterized.

2.5. Optic nerve analysis by GC-MS

The analysis of the derivatized extracts was performed with a GC instrument (7890A, Agilent Technologies) coupled to an inert mass spectrometer with triple-Axis detector (5975C, Agilent Technologies). The injection volume of derivatized samples was set at 2 µL using an autosampler (7693, Agilent Technologies). Samples were automatically injected in split mode, with a split ratio 1:10, into an Agilent deactivated glass wool split liner. Separation of the compounds was achieved using a 10 m J&W pre-column (Agilent Technologies) integrated with a 122−5332G column: DB5-MS 30m length, 0.25 mm i.d. and 0.25 µm film consisting of 95% dimethyl/5% diphenyl polysiloxane (Agilent Technologies). Helium was used as the carrier gas with a constant flow rate of 1 mL/min. The lock of the retention time (RTL) relative to the internal standard (methyl stearate C18) peak at 19.66 minutes was performed. The chromatographic separation consisted on temperature gradient for the column oven programmed at 60 ℃ (maintained for 1 minute), then raised by 10 ℃/min until it reached 325 ℃, and was held at this temperature for 10 minutes before cooling down. The injector and the transfer line temperatures were set at 250 ℃ and 280 ℃, respectively. MS system: the electron impact ionization operating parameters were set as follows: filament source temperature, 230 ℃; electron ionization energy, 70 eV. Mass spectra acquisition range was set at 50 to 600 m/z at a scan rate of 2 spectra/s. For retention index determination, a mixture of *n*-alkanes (C8-C28) dissolved in *n*-hexane was run prior to the samples. Data were acquired using the Agilent MSD ChemStation Software (Agilent Technologies).

2.6. GC-MS data treatment

Total ion chromatograms (TICs) obtained after the analysis were inspected based on both quality of the chromatograms and internal standard signals. First, samples were processed with MassHunter Workstation GC/MS Translator software version B.04.01, in order to made them compatible with the MassHunter Quantitative data analysis version B.08.00. The resulting data

files were exported to Agilent MassHunter Unknowns Analysis Tool 7.0 for the deconvolution process and metabolite identification of raw data collected by GC-MS analysis. In order to obtain a chemical identity for the compounds, the software executed a search against two target libraries: Fiehn library version 2008 and the CEMBIO in-house spectral library and always by comparing both retention time (RT) and spectra extracted during the deconvolution against each compound included in the library. In addition, a commercial spectral library — NIST (National Institute of Standards and Technology) library 2.2 version 2014 — was used for comparing non-identified compounds. Those metabolites with spectrum score higher than 80% and concordant retention index (*n*-alkane scale) were putatively identified according to NIST. Data obtained by the Unknown Analysis Tool were aligned using MassProfiler Professional B.12.1 (Agilent Technologies). Then, Agilent MassHunter Quantitative Analysis version B.08.00 was used for the assignment of the target and qualifiers ions and peak area integration. Prior to the statistical analysis, sample areas were normalized by pentadecanoic acid (IS) abundance in order to minimize the response variability coming from the instrument, and then each sample was normalized by the amount of protein per optic chiasm, expressed in micrograms (µg). Finally, data were filtered by the coefficient of signal variation (CV) in QCs, considering as acceptable values lower than 30%.

2.7. Statistical analysis

Targeted metabolomics

After the analysis, data were collected and reprocessed as previously described, followed by the univariate statistical analysis (UVDA). For this purpose, the normality of data was assessed by Shapiro-Wilk test and then Student´s *t* test ($p \leq 0.05$) using MATLAB (R2015a, MathWorks), with unpaired unequal variance assumed, was performed, to determine whether the mean values of the two groups were different for lactic acid and pyruvic acid. Finally, in order to control the false discovery rate at level $\alpha = 0.05$, Benjamini–Hochberg correction test were employed [14].

Non-targeted metabolomics

To investigate differences in the global profile between the groups, both univariate (UVDA) and multivariate data analysis (MVDA) were assayed. The UVDA was performed following the same statistical approach as for targeted metabolomics, to test each individual metabolite in the samples. For MVDA, processed data were imported into SIMCA version 14 (Umetrics, Umeå, Sweden). Initially, unsupervised principal component analysis (PCA) plot was applied considering all samples from both groups including QC samples to observe the natural grouping of samples and verify the clustering of QCs, revealing the robustness and stability of the analytical procedure. In order to investigate the compounds that account for the PCA separation,

supervised partial least square discriminant analysis (PLS-DA) model was plotted. Finally, OPLS-DA models for the comparison were obtained. The fitness and prediction capabilities of each model were assessed by the explained variance (R^2) and the predicted variance (Q^2), respectively, supplied by the software. Finally, statistically significant variables were selected on the basis of the variable importance in the project (VIP) value and jackknifing confidence interval resulting from the OPLS-DA model[15]. Since OPLS-DA method has a high tendency to over-fit models to the data, the model built was obtained was validated applying cross-validation strategy in order to avoid the risk of overfitting and test the predictability of the statistical model, leaving 1/3 of the samples out per group and calculating the percentage of samples correctly classified into their respective groups [16].

3. Validation Study

The method for extraction and quantitation of lactic and pyruvic acid in optic nerve samples was validated in terms of selectivity, linearity, limits of detection and quantitation (LOD and LOQ, respectively), recovery, instrumental precision and method precision (both with standards and samples) for GC-MS platform.

Linearity, LOD and LOQ

The linearity of the relative response for standards was tested based on the three replicates of six different concentration levels of standard solutions, covering the expected values oscillating between 10% and 200% of mean values obtained in preliminary measurements with real samples.

The LOD and LOQ were determined at the lowest concentration point of linearity by using signal-to-noise ratio (S/N)= 3 and 10, respectively.

Recovery

The recovery of the two analytes was evaluated with samples spiked with known standard solutions. This parameter was tested at four different levels of concentration (50%, 100%, 150%, 200%) and the analysis was repeated three times for each concentration. The regression coefficients of these standard addition calibrations were calculated. Besides the recovery of the analytes was reported by comparing the added concentrations with the experimental ones.

Precision

The instrumental precision of the method was evaluated based on the consistency of instrumental response for a given analyte in the midrange of the calibration curve. It was calculated by consecutive injections (n= 10) of a homogeneous standard solution. The intra-day precision of the method was assessed by injecting individual preparations of standards and

samples (n=7 and n=6, respectively) in the midrange of the calibration curve. Inter-day (n= 12) precision was tested in the same way, but repeating the experiment on a different day, with a new no-defrosted optic nerve pool.

Working Solutions and Standards

Individual stock solutions of lactic acid, pyruvic acid, pentadecanoic acid (IS), and Methyl stearate (IS) were prepared in methanol and stored at -20°C. From these solutions, an intermediate solution of each compound was prepared and stored at 4°C during the working week and these solutions were appropriately diluted on the day of the analysis.

4. RESULTS

4.1. Method validation

The main objectives of this study were the development of a method for the absolute quantitation of lactic and pyruvic acid in optic nerve tissue samples and to validate the method as a robust, sensitive, and reproducible along with the characterization of its metabolic profile by GC-MS technique. During the validation process, the correlation coefficients obtained fitted the linear model ($r \geq 0.990$) for both metabolites and no bias was found for lactic acid since the confidence limit calculated for the intercept included the zero but for pyruvic acid slight bias was found due to the lower variability of the data and without further consequences.

Recoveries were 100.4% for pyruvic acid and 106.9% for lactic acid, with a RSD of 6.6% and 6.5%, respectively (n = 12). For standards, instrumental precision (n = 10) was tested for a constant response of IS and were 1.2 % to 3.4 % respectively. Intra-day precision for standards (n = 7) ranged from 3.4 % to 6.4 %. RSD for intra-day precision were calculated by analyzing the same assay 6 aliquots independently prepared from the pool of sample. The daily RSD ranged from 5.9 % to 7.3 %, and the values obtained in the inter-day precision study were from 6.1 % to 9.5 % in different days (n = 12).

For each compound, the theoretical LOD calculated based on the IUPAC method ranged from 2.5×10^{-4} mM in solution equivalent to 0.012 µg/sample, and the LOQ was in the range 8.4×10^{-4} mM equivalent to 0.042 µg/sample. These values were found to be lower than the lowest value of their respective range of standards. All these validation parameters and their results are summarized in Table 1.

TABLE 1

296 **4.2. Targeted metabolomics**

297 The validated extraction method for quantitation of lactic acid and pyruvic acid in optic nerve
298 tissue by GC-MS was employed for the absolute quantitation of these two metabolites in the 18
299 samples corresponding to the NVD mice group (n = 9) and WT group (n = 9).

300 For this purpose, linear regressions were assayed for both metabolites using pentadecanoic acid
301 as IS covering the range of expected concentration values. The linearity of each analyte standard
302 was evaluated, obtaining a correlation coefficient, r > 0.997 and r > 0.995 for lactic acid and
303 pyruvic acid, respectively. After the univariate statistical analysis for the comparison of the two
304 groups, the p values obtained for lactic acid and pyruvic acid were 0.0049, and 6.48×10^{-4},
305 respectively resulting statistically significant their differences. These results are represented in
306 Fig. 2.

307 FIGURE 2

308 **4.3. Non-targeted metabolomics**

309 For the non-targeted metabolomics approach, the method was employed for the analysis by GC-
310 MS of the optic nerve samples belonging to the NVD group (n = 9) and WT group (n = 9).

311 After GC-MS analysis and data pretreatment, 109 entities were obtained after deconvolution,
312 and alignment and after data normalization and filtering, 79 of them were annotated
313 compounds with RSDs below 30% in the QC samples. This data set was used for further analyses.
314 Concerning to the robustness of the methodology, the initial PCA plot showed the QC samples
315 tightly cluster, determining the stability and reproducibility of the system. PLS-DA plot showed
316 that samples have a clear tendency to gather into their respective groups, suggesting that the
317 metabolites levels change due to the mutation present in the NVD group respecting the WT
318 group. These differences were evaluated by an OPLS-DA model. Regarding to the quality of the
319 multivariate models obtained, PCA plot presents a quality of variance explained and predicted
320 variance of $R^2 = 0.683$, $Q^2 = 0.545$; and PLS-DA plot presents $R^2 = 0.976$, $Q^2 = 0.880$. Finally, OPLS-
321 DA model presents $aR^2 = 0.998$, $Q^2 = 0.929$, with a percentage of samples correctly classified of
322 97.22% ± 6.8 SD, after cross-validation test. All the models were built with UV-scaling. Plots for
323 each model are represented in Fig. 3.

324 Additionally, univariate statistical analysis was performed simultaneously with multivariate
325 statistical analysis, and on the basis of the VIP threshold (VIP ≥ 1), jackknifing confidence interval
326 not including 0, and the Student's t test p value ($p < 0.05$) corrected by Benjamini–Hochberg
327 test, 34 metabolites were found as statistically significant when comparing NVD *vs* WT. Finally,
328 fold change was calculated for each metabolite to evaluate the positive or negative trend of

their levels regarding to the control group. As it can be observed in Table 2, an overall positive trend was found in all the metabolites obtained after both statistical analyses.

FIGURE 3

TABLE 2

4.4. Characterization of the metabolite profile

Chromatographic profiles obtained after GC-MS analysis were characterized by using the standard "Fiehn metabolomics retention time lock (RTL)" method. At the end of the process, 94 peaks were assigned to the optic nerve profile. Amino acids, carboxylic, dicarboxylic, and tricarboxylic acids, hydroxy acids, pyrimidines, purines and purine nucleosides, sugars, cholesterol, amines, carbohydrates, glycerolipids, glycerophospholipids, and fatty acids among other metabolite classes can be distinguished across the profile. Most of the metabolites identified were derived from the endogenous metabolism of the optic nerve tissue, and are known to be involved in several metabolic pathways. Cholesterol can be observed as the highest peak in the chromatogram, followed by *myo*-inositol. This is consistent with the fact that cholesterol is present in a high abundance in the nervous system as the major architectural component of compact myelin. Lipid composition of nervous tissues ranged from 50 % to 60 % of their dry weight. Together with cholesterol, different fatty acid classes were found at lower levels, divided in saturated fatty acids (SFA) caproic acid (C6:0), palmitic acid (C16:0), stearic acid (C18:0), and arachidic acid (C20:0); monounsaturated fatty acid (MUFA) oleic acid (C 18:1 cis-9); and polyunsaturated fatty acids (PUFA) including linoleic acid (C18:2 ω-6), and arachidonic acid (C20:4 ω-6). Regarding to *myo*-inositol, its levels as a free form are higher in nerves than in any other tissues [18]. It is considered as glial cell marker and its abundance is also higher in glial cells than in neurons [19, 20]. Fructose and mannose are considered as alternative energy substrates. Optic nerve tissue can supply a glucose deficit with these two sugars to achieve the generation of compound action potentials (CAPs) [21]. Along with cholesterol and *myo*-inositol, acetoacetate, lactic acid, phosphoric acid, leucine, and glycerol peaks also domain the profile. Some of the compounds here described have been previously reported in human, rat and mouse optic nerve tissue by different analytical approaches [12, 22-24], but to our knowledge, this is the first time that the whole metabolomic profile of mouse optic nerve has been characterized by GC-MS analysis. The 94 compounds assigned along the TIC obtained after the GC-MS analysis are presented in Fig. 4 and Table 3

FIGURE 4

TABLE3

4.5. Metabolic pathway analysis

Once the method for the analysis of optic nerve samples by GC-MS was validated and then used for the non-targeted metabolomics study, the visualization and interpretation of the connections among the 34 metabolites resulted as statistically significant through their metabolomic networks were achieved using MetScape, a plug-in of Cytoscape [32]. The metabolomic network obtained remarks the main metabolic interconnections, resulting in an integration of the metabolomics experimental results with biological knowledge[33]. In this way, the principal metabolic pathways affected by the NVD mutation presented in the optic nerve tissue were easily identified. The organism selected in the KEGG database included in the software was *Mus musculus*, aiming to increase the specificity of the results. In the Fig.5, the dark red hexagons represent the significant metabolites obtained in our analysis, while the light red hexagons were designated to the intermediary metabolites that are known to be involved within each metabolic reaction, connecting through them the different metabolic pathways that resulted affected. Additionally, according to the altered metabolites listed in Table 2, a quantitative enrichment analysis (QEA) was built with MetaboAnalyst 3.0 (http://www.metaboanalyst.ca) to distinguish whether any certain identified pathway is more represented than the others, based on their *p* values and the fold enrichment. The ratio of altered metabolites and the total number of metabolites involved in the pathway are also represented in the table supplied [34, 35].

The interconnections of 26 metabolic pathways are represented in the metabolomic network graphic, including Bile acid biosynthesis, β-alanine metabolism, Galactose metabolism, Glycerophospholipid metabolism, Glycine, serine, alanine and threonine metabolism, Glycolysis and Gluconeogenesis, Glycosphingolipid metabolism, Methionine and cysteine metabolism, Pyrimidine metabolism, Squalene and cholesterol biosynthesis, TCA cycle, Urea cycle, Arginine, proline, glutamate, aspartate and asparagine metabolism, Valine, leucine and isoleucine degradation, among others.

However, 22 metabolite sets were enriched in the optic nerve tissue of NVD mice group comparing with the WT group, with a *p*FDR < 0.05, considering just pathways matching more than 2 metabolites in the pathway (Table 4). Based on the results reflected in the quantitative enrichment analysis, the most enriched pathway related to the NVD mutation is the pyrimidine metabolism (*p*FDR = 0.0014), counting with 4 altered metabolites of its 36 total compounds, together with the galactose pathway (*p*FDR = 0.0014), with 2 of the 25 compounds that are integrated in this pathway. Additionally, different enriched metabolic pathways can be found in the table, as the urea cycle (*p*FDR = 0.0076) with 7 of the 20 compounds that conform this cycle, followed by arginine and proline metabolism (*p*FDR = 0.0076) with 6 enriched metabolites of its

26. Alanine, glutamic acid and pyruvic acid encompass the 50% of the metabolites that form the alanine metabolism (*p*FDR = 0.0076), and together with the protein biosynthesis (*p*FDR = 0.0076), which presents a 63% of its metabolites altered, are also strongly affected in the optic nerve metabolism due to the mutation present in these mouse model.

FIGURE 5

TABLE 4

5. DISCUSSION

Optic neuropathies represent an important cause of acute to chronic visual impairment and blindness. Alterations in the metabolism of the neural system lead to serious visual-neurologic pathologies such as Leber's Hereditary Optic Neuropathy, Kjer's syndrome, Friederich Ataxia or Leigh's Syndrome [25, 26]. A common feature presented in the pathophysiology of these diseases is the genetic or acquired mitochondrial dysfunction, which produces the selective loss of retinal ganglion cells (RGCs) and contributes to the optic nerve degeneration [36]. Mitochondria produce energy from different substrates; thus, the accumulation of energy substrates, including pyruvic acid, branched-chain amino acids (BCAAs), and fatty acids, and their by-products such as alanine, ornithine, or lactic acid that we observed in this NDV mice model might indicate a mitochondrial dysfunction.

The optic nerve is the principal myelinated tract of the Central Nervous System (CNS) and is formed by two different types of cells: neurons, excitable cells responsible for the transmission of the nerve impulse and glial cells (astrocytes, oligodendrocytes, microglia), that confer mainly metabolic support to neurons [27, 28]. In a certain way, a correct metabolic coupling between oligodendrocytes, astrocytes and neurons is necessary for the proper functioning of the neural circuits in the optic nerve [29-31]. Specifically, two essential metabolites for the appropriate optic nerve function are lactate and pyruvate. Physiologically, neurons transform lactate into pyruvate and degrade it in the mitochondria in order to obtain energy. Therefore, alterations in neuronal and glia metabolism lead to an imbalance in the levels of lactate and pyruvate in neuronal circuits. Thus, the unavailability of energy production among the cell types could explain the accumulation of lactate and pyruvate in our mutant mouse´s optic nerve due to the incapacity of them being degraded, thus causing a pathological condition.

Regarding to the enrichment of amino acids such as alanine, glycine, threonine, serine, phenylalanine and leucine suggests an increase in protein catalysis, possibly due to their oxidation. This correlates with the high measures of aminomalonic acid and hypotaurine, both seen in stress-like situations induced by mitochondrial dysfunction [37, 38].

Valine, leucine, and isoleucine are the three essential BAAs. The transport of these three metabolites, together with other amino acids (phenylalanine, tryptophan, methionine, tyrosine, histidine, and threonine) into the brain and other organs is possible through the presence of the L1-neutral amino acid transporter (LAT1) [39]. In consequence, amino acid uptake by the brain and the neurotransmitters synthesis will be determined by the relative concentration of each amino acid and the competition among them for the same transporter. In fact, Leu plays a key role in mammals' metabolism. Neurons need a constant supply of glutamate, which is oxidized not only by neurons but also by the glia cells. BCAAs, and in particular Leu, are a source of nitrogen donors (-NH_2) for glutamate synthesis [40]. The deamination of Leu, which is obtained from the blood stream, takes place mainly in the astrocytes, leading to glutamate. Then glutamate is converted into glutamine through the action of the enzyme glutamine synthetase (GS), which is the major glutamate-forming enzyme located in astroglial cells and also plays a critical role in the ammonia assimilation [41]. Then, when glutamine is transported to the neurons, can be transformed to glutamate to close the metabolic route. In consequence, one molecule of ammonia is released and must be transported back to the astrocyte for the detoxification process. If the mechanism of recycling ammonia is not working properly and gets accumulation in neuronal tissue, it might cause neurotoxicity by affecting metabolic pathways of several amino acids including neurotransmitters, and can induce oxidative stress, alterations in the nitric oxide synthesis, mitochondrial permeability transition and signal transduction pathways. These events might induce neuronal loss, axonal impairment and deficiency of dendritic growth [42]. A deficiency in the activity of the enzyme GS could explain the alterations observed in the glutamate metabolism pathway and in the ammonia recycling process displayed by the QEA, together with the accumulation of urea in the optic nerve. The increment of creatinine levels could be explained as consequence of the up-regulation of several metabolites involved in the urea cycle, from which this metabolite derives. Additionally, an increment of glycine was detected and it is linked with urea and creatinine through the creatine/creatinine metabolism and its coupling to the urea cycle and the catabolism of L-arginine and L-ornithine. The urea cycle is one of the pathways involved in the detoxification process of ammonia [43]. It involves a set of biochemical steps in which nitrogenous waste products coming from protein and amino acid breakdown are removed by their conversion into urea. Citrulline and aspartic acid are substrates also for urea synthesis, giving fumaric acid, and ornithine as intermediate metabolites. Fumaric acid is directed into the citric acid cycle, while ornithine will be the starting point for the synthesis of other metabolites found altered in this study, including glutamate.

Therefore, we hypothesize that in order to keep physiological energy levels, the optic nerve cell needs to modify its metabolism degrading proteins and so generating the observed amino acid excess. As a consequence of the degradation of proteins, urea is over-generated (and also

ornithine and other intermediate metabolites). The connection between these metabolic pathways is represented in Fig. 6.

Additionally, N-acetyl-aspartate (NAA), an acetyl group donor from aspartic acid, was also increased in NVD mice. This metabolite is present at high concentrations in the neuronal tissue of brain mammals, being second only to glutamate in terms of the free amino acid derivative. However, it is practically undetectable in other tissues [44]. It is located predominantly within the cellular matrix in the nerve cells. The enzyme responsible for its synthesis, the *N*-acetyl transferase, is exclusively present in nervous tissue, more specifically, in the mitochondrial fraction [24, 45]. On the other hand, the enzyme in charge of its degradation, the aspartoacylase (ASPA), has been found expressed only in oligodendrocytes [46]. Despite of the fact that its role still remains unclear, it is suggested that NAA, together with NAAG, is involved in cellular signaling mechanisms and plays a key role in the regulation of the brain cells interconnections and the maintenance of the nervous system. NAA could also indicate the neuronal viability in many neurodegenerative diseases, including axonal pathologies [24]. The increased levels of NAA in the optic nerve tissue could be produced by a reduction of the catabolic enzyme activity, and this might lead to a demyelination process, which is a common feature in the Canavan disease (CD). The NAA increment can also generate an up-regulation of nitric oxide levels causing oxidative stress, genotoxicity and protein interaction, that contribute to neurodegenerative processes [47]. Additionally, since NAA is synthesized in the mitochondria, its increment could be also explained by the higher levels of pyruvic acid present in the optic nerve of NVD mice, since this relationship has been previously described in mitochondria from brain rats [48].

FIGURE 6

6. CONCLUSIONS

A sensitive, rapid, and simple one single-phase method for the extraction and analysis of metabolites in optic nerve tissue samples by GC-MS is presented. The method was validated for the quantitation of two specific metabolites, lactic acid and pyruvic acid, in terms of linearity, recovery, sensitivity, and precision Based on our results, the method was found to be reliable for the targeted and non-targeted metabolomics analysis of the optic nerve samples. The whole metabolite profile has been characterized and 94 peaks were identified. Employing the validated method, lactic acid and pyruvic acid were quantified in the optic nerve samples of NVD and the transgene-negative WT littermates used as the control group. Moreover, considering the results of multivariate statistical analysis models obtained, a good classification of samples was observed, reflecting the effects of the NVD mutation in the optic nerve. Besides, 34 metabolites

were annotated as potential biomarkers when comparing both groups, including the two targeted metabolites lactic acid and pyruvic acid. Finally, after obtaining the metabolic network map where these metabolites were involved, the interconnections of 26 different pathways were found, complemented with the quantitative enrichment analysis, which reflected 22 enriched pathways with a *p*FDR < 0.05. Finally, the combination of target and untargeted metabolomic study of optic nerve samples by GC-MS have confirmed alterations in the levels of lactate and pyruvate among other metabolites, supporting this animal model to be suited for the study of optic neuropathies.

ACKNOWLEDGMENTS

The authors gratefully acknowledge the financial support from the Spanish Ministry of Economy, Industry and Competitiveness (Grants CTQ2014-55279-R to CB and AG and Grant BFU2015-64829-R to BC), and Fundación Universitaria San Pablo CEU (CGR PhD fellowship).

REFERENCES

[1] J.H. Wang, J. Byun, S. Pennathur, Analytical approaches to metabolomics and applications to systems biology, Seminars in nephrology, Elsevier, 2010, pp. 500-511.

[2] O. Fiehn, Metabolomics - the link between genotypes and phenotypes, Plant Molecular Biology 48(1-2) (2002) 155-171.

[3] J.K. Nicholson, J.C. Lindon, E. Holmes, 'Metabonomics': understanding the metabolic responses of living systems to pathophysiological stimuli via multivariate statistical analysis of biological NMR spectroscopic data, Xenobiotica 29(11) (1999) 1181-1189.

[4] C. Menni, J. Zierer, A.M. Valdes, T.D. Spector, Mixing omics: combining genetics and metabolomics to study rheumatic diseases, Nature Reviews Rheumatology 13(3) (2017) 174-181.

[5] G.J. Patti, O. Yanes, G. Siuzdak, Metabolomics: the apogee of the omics trilogy, Nature Reviews Molecular Cell Biology 13(4) (2012) 263-269.

[6] N. Gehlenborg, S.I. O'Donoghue, N.S. Baliga, A. Goesmann, M.A. Hibbs, H. Kitano, O. Kohlbacher, H. Neuweger, R. Schneider, D. Tenenbaum, A.-C. Gavin, Visualization of omics data for systems biology, Nature Methods 7(3) (2010) S56-S68.

[7] J. Haggarty, K.E.V. Burgess, Recent advances in liquid and gas chromatography methodology for extending coverage of the metabolome, Current Opinion in Biotechnology 43 (2017) 77-85.

[8] K.K. Pasikanti, P.C. Ho, E.C.Y. Chan, Gas chromatography/mass spectrometry in metabolic profiling of biological fluids, Journal of Chromatography B-Analytical Technologies in the Biomedical and Life Sciences 871(2) (2008) 202-211.

[9] K.A.Z. Berry, W.C. Gordon, R.C. Murphy, N.G. Bazan, Spatial organization of lipids in the human retina and optic nerve by MALDI imaging mass spectrometry, Journal of lipid research 55(3) (2014) 504-515.

[10] D.M. Anderson, J.M. Spraggins, K.L. Rose, K.L. Schey, High spatial resolution imaging mass spectrometry of human optic nerve lipids and proteins, Journal of the American Society for Mass Spectrometry 26(6) (2015) 940-947.

[11] C. Balaratnasingam, W.H. Morgan, V. Johnstone, S.J. Cringle, D.-Y. Yu, Heterogeneous distribution of axonal cytoskeleton proteins in the human optic nerve, Investigative ophthalmology & visual science 50(6) (2009) 2824-2838.

[12] N. Acar, O. Berdeaux, S. Gregoire, S. Cabaret, L. Martine, P. Gain, G. Thuret, C.P. Creuzot-Garcher, A.M. Bron, L. Bretillon, Lipid Composition of the Human Eye: Are Red Blood Cells a Good Mirror of Retinal and Optic Nerve Fatty Acids?, Plos One 7(4) (2012).

[13] K. Nagy, V.V. Brahmbhatt, O. Berdeaux, L. Bretillon, F. Destaillats, N. Acar, Comparative study of serine-plasmalogens in human retina and optic nerve: identification of atypical species with odd carbon chains, Journal of lipid research 53(4) (2012) 776-783.

[14] M. Vinaixa, S. Samino, I. Saez, J. Duran, J.J. Guinovart, O. Yanes, A Guideline to Univariate Statistical Analysis for LC/MS-Based Untargeted Metabolomics-Derived Data, Metabolites 2(4) (2012) 775-95.

[15] P. Zhang, W.T. Zhu, D.Z. Wang, J. Yan, Y. Wang, L. He, Enantioselective Effects of Metalaxyl Enantiomers on Breast Cancer Cells Metabolic Profiling Using HPLC-QTOF-Based Metabolomics, International Journal of Molecular Sciences 18(1) (2017).

[16] B. Worley, R. Powers, Multivariate Analysis in Metabolomics, Current Metabolomics 1(1) (2013) 92-107.

[18] H. Kusama, M.A. Stewart, LEVELS OF MYO-INOSITOL IN NORMAL AND DEGENERATING PERIPHERAL NERVE, Journal of Neurochemistry 17(3) (1970) 317-&.

[19] L.J. Wu, Z.H. Tang, X.Y. Feng, X.H. Sun, W. Qian, J. Wang, L.X. Jin, J.X. Jiang, Y.F. Zhong, Metabolic Changes in the Bilateral Visual Cortex of the Monocular Blind Macaque: A Multi-Voxel Proton Magnetic Resonance Spectroscopy Study, Neurochemical Research 42(2) (2017) 697-708.

[20] J.-K. Choi, A. Dedeoglu, B.G. Jenkins, Application of MRS to mouse models of neurodegenerative illness, Nmr in Biomedicine 20(3) (2007) 216-237.
[21] P.P. Dzeja, A. Terzic, Handbook of Neurochemistry and Molecular Neurobiology: Brain Energetics. Integration of Molecular and Cellular Processes, Springer US, 2007.
[22] J.M.C. de la Barca, G. Simard, E. Sarzi, T. Chaumette, G. Rousseau, S. Chupin, C. Gadras, L. Tessier, M. Ferre, A. Chevrollier, V. Desquiret-Dumas, N. Gueguen, S. Leruez, C. Verny, D. Milea, D. Bonneau, P. Amati-Bonneau, V. Procaccio, C. Hamel, G. Lenaers, P. Reynier, D. Prunier-Mirebeau, Targeted Metabolomics Reveals Early Dominant Optic Atrophy Signature in Optic Nerves of Opa1(delTTAG/+) Mice, Investigative Ophthalmology & Visual Science 58(2) (2017).
[23] C.L. Florian, S.R. Williams, K.K. Bhakoo, M.D. Noble, Regional and developmental variations in metabolite concentration in the rat brain and eye: A study using H-1 NMR spectroscopy and high performance liquid chromatography, Neurochemical Research 21(9) (1996) 1065-1074.
[24] C. Bjartmar, J. Battistuta, N. Terada, E. Dupree, B.D. Trapp, N-acetylaspartate is an axon-specific marker of mature white matter in vivo: A biochemical and immunohistochemical study on the rat optic nerve, Annals of Neurology 51(1) (2002) 51-58.
[25] V. Carelli, F.N. Ross-Cisneros, A.A. Sadun, Optic nerve degeneration and mitochondrial dysfunction: genetic and acquired optic neuropathies, Neurochemistry international 40(6) (2002) 573-584.
[26] N. Howell, Leber hereditary optic neuropathy: respiratory chain dysfunction and degeneration of the optic nerve, Vision research 38(10) (1998) 1495-1504.
[27] M. Tsacopoulos, P.J. Magistretti, Metabolic coupling between glia and neurons, Journal of Neuroscience 16(3) (1996) 877-885.
[28] A.M. Brown, S.B. Tekkök, B.R. Ransom, Energy transfer from astrocytes to axons: the role of CNS glycogen, Neurochemistry international 45(4) (2004) 529-536.
[29] K.-A. Nave, B.D. Trapp, Axon-glial signaling and the glial support of axon function, Annu. Rev. Neurosci. 31 (2008) 535-561.
[30] S.B. Tekkök, A.M. Brown, R. Westenbroek, L. Pellerin, B.R. Ransom, Transfer of glycogen-derived lactate from astrocytes to axons via specific monocarboxylate transporters supports mouse optic nerve activity, Journal of neuroscience research 81(5) (2005) 644-652.
[31] Y. Lee, B.M. Morrison, Y. Li, S. Lengacher, M.H. Farah, P.N. Hoffman, Y. Liu, A. Tsingalia, L. Jin, P.-W. Zhang, Oligodendroglia metabolically support axons and contribute to neurodegeneration, Nature 487(7408) (2012) 443-448.
[32] P. Shannon, A. Markiel, O. Ozier, N.S. Baliga, J.T. Wang, D. Ramage, N. Amin, B. Schwikowski, T. Ideker, Cytoscape: A software environment for integrated models of biomolecular interaction networks, Genome Research 13(11) (2003) 2498-2504.
[33] J. Gao, V.G. Tarcea, A. Karnovsky, B.R. Mirel, T.E. Weymouth, C.W. Beecher, J.D. Cavalcoli, B.D. Athey, G.S. Omenn, C.F. Burant, H.V. Jagadish, Metscape: a Cytoscape plug-in for visualizing and interpreting metabolomic data in the context of human metabolic networks, Bioinformatics 26(7) (2010) 971-973.
[34] S.C. Booth, A.M. Weljie, R.J. Turner, Computational tools for the secondary analysis of metabolomics experiments, Computational and structural biotechnology journal 4 (2013) e201301003-e201301003.
[35] J. Xia, D.S. Wishart, MSEA: a web-based tool to identify biologically meaningful patterns in quantitative metabolomic data, Nucleic acids research 38(suppl_2) (2010) W71-W77.
[36] P. Yu-Wai-Man, M. Votruba, F. Burté, C. La Morgia, P. Barboni, V. Carelli, A neurodegenerative perspective on mitochondrial optic neuropathies, Acta neuropathologica 132(6) (2016) 789-806.
[37] H. Pasantes-Morales, C. Cruz, Taurine and hypotaurine inhibit light-induced lipid peroxidation and protect rod outer segment structure, Brain research 330(1) (1985) 154-157.
[38] R.L. Levine, Carbonyl modified proteins in cellular regulation, aging, and disease 2, 3, Free Radical Biology and Medicine 32(9) (2002) 790-796.

[39] I. Manoli, C. Venditti, Disorders of branched chain amino acid metabolism, Translational Science of Rare Diseases 1(2) (2016) 91-110.
[40] M. Yudkoff, Y. Daikhin, I. Nissim, O. Horyn, B. Luhovyy, A. Lazarow, I. Nissim, Brain amino acid requirements and toxicity: the example of leucine, The Journal of nutrition 135(6) (2005) 1531S-1538S.
[41] C. Oliver, P. Starke-Reed, E. Stadtman, G. Liu, J. Carney, R. Floyd, Oxidative damage to brain proteins, loss of glutamine synthetase activity, and production of free radicals during ischemia/reperfusion-induced injury to gerbil brain, Proceedings of the National Academy of Sciences 87(13) (1990) 5144-5147.
[42] L. Cagnon, O. Braissant, Hyperammonemia-induced toxicity for the developing central nervous system, Brain research reviews 56(1) (2007) 183-197.
[43] J.W. Kemp, D.M. Woodbury, Synthesis of urea-cycle intermediates from citrulline in brain, Biochimica et Biophysica Acta (BBA)-General Subjects 111(1) (1965) 23-31.
[44] H.D. Yan, K. Ishihara, T. Serikawa, M. Sasa, Activation by N-acetyl-L-aspartate of acutely dissociated hippocampal neurons in rats via metabotropic glutamate receptors, Epilepsia 44(9) (2003) 1153-1159.
[45] J. Clark, N-acetyl aspartate: a marker for neuronal loss or mitochondrial dysfunction, Developmental neuroscience 20(4-5) (1998) 271-276.
[46] M.H. Baslow, R.F. Suckow, V. Sapirstein, B. Hungund, Expression of aspartoacylase activity in cultured rat macroglial cells is limited to oligodendrocytes, Journal of Molecular Neuroscience 13(1) (1999) 47-53.
[47] S. Surendran, M. Bhatnagar, Upregulation of N-acetylaspartic acid induces oxidative stress to contribute in disease pathophysiology, International Journal of Neuroscience 121(6) (2011) 305-309.
[48] T.B. Patel, J.B. Clark, Synthesis of N-acetyl-L-aspartate by rat brain mitochondria and its involvement in mitochondrial/cytosolic carbon transport, Biochemical Journal 184(3) (1979) 539-546.

647 TABLES
648

Validation parameters	Lactic acid	Pyruvic acid
Linearity		
Slope	9.04 ± 0.73	4.31 ± 0.32
Intercept	0.093 ± 0.112	$1.6x10^{-3}$ ± 7.20^{-4}
r	0.991	0.993
Range (mM)	0.015 - 0.300	$2.2x10^{-4}$ - $4.4x10^{-3}$
Range (µg/sample)	0.135-2.027	$1.9x10^{-3}$ - $3.9x10^{-2}$
Range (µg/ µg protein)	0.00105 - 0.0158	$1.5\ x10^{-5}$ - $3.04\ x10^{-4}$
Recovery		
(%)	106.9	100.4
RSD (%)	6.5	6.6
Method precision with standards		
Instrumental precision (n=10), %RSD	1.2	3.4
Intra-day (n=7), %RSD	3.4	6.4
Method precision with sample		
Intra-day (n=6), %RSD	5.9	7.3
Inter-day (n=12), %RSD	6.1	9.5
LOD (µg/ µg protein)	$9.4\ x10^{-5}$	$1.95x10^{-6}$
LOQ (µg/ µg protein)	$3.4\ x10^{-4}$	$6.5x10^{-6}$

649
650

651 Table 1. Validation results for Lactic acid and Pyruvic acid in mouse optic nerve tissue obtained
652 with the optimized method by GC-MS analysis.

653

Compound	Mass (DB)	Molecular formula	RT (min)	*p* Value	*p*BH	CV	VIP	JK	% CHANGE	FC	HMDB CODE
Alpha-keto acids and derivatives											
Pyruvic acid	88.0160	$C_3H_4O_3$	6.67	$4.1x10^{-5}$	$6.5x10^{-4}$	1.6	1.19	YES	58.9	1.59	HMDB00243
Amino acids, peptides, and analogues											
Alanine	89.0476	$C_3H_7NO_2$	7.45	0.011	0.025	6.9	1.07	YES	40.3	1.40	HMDB00161
Glycine	75.0320	$C_2H_5NO_2$	7.73	0.0028	0.0096	4.8	1.10	YES	43.5	1.44	HMDB00123
Leucine	131.0946	$C_6H_{13}NO_2$	8.25	$1.6x10^{-4}$	0.0017	6.4	1.21	YES	34.7	1.35	HMDB00687
Serine	105.0425	$C_3H_7NO_3$	9.67	0.019	0.032	3.4	1.08	YES	44.0	1.44	HMDB00187
Isoleucine	131.0946	$C_6H_{13}NO_2$	10.15	0.0056	0.018	3.5	1.08	YES	30.7	1.31	HMDB00172
Threonine	119.0582	$C_4H_9NO_3$	10.18	0.014	0.027	4.7	1.05	YES	45.4	1.45	HMDB00167
β-Alanine	89.0477	$C_3H_7NO_2$	10.35	0.031	0.047	2.6	0.94	YES	28.5	1.28	HMDB00056
Trans-4-hydroxy-L-proline	131.0582	$C_5H_9NO_3$	13.14	0.019	0.032	4.3	1.02	YES	29.9	1.30	HMDB00725
Glutamic acid	147.0532	$C_5H_9NO_4$	13.29	0.014	0.027	3.1	1.09	YES	39.8	1.40	HMDB00148
Ornithine	132.0898	$C_5H_{12}N_2O_2$	14.33	0.014	0.027	13.5	1.07	YES	50.9	1.51	HMDB00214
Tyrosine	181.0739	$C_9H_{11}NO_3$	17.30	0.011	0.025	6.1	0.99	YES	30.0	1.30	HMDB00158
Benzoic acids and derivatives											
Benzoic acid	122.0368	$C_7H_6O_2$	9.57	$2.9x10^{-4}$	0.0023	7.6	1.20	YES	41.1	1.41	HMDB01870
Carbohydrates and carbohydrate conjugates											
Glycerol	92.0473	$C_3H_8O_3$	9.87	$2.9x10^{-4}$	0.0023	5.4	1.22	YES	34.1	1.34	HMDB00131
Carboxylic acids and derivatives											
Aspartic acid	133.0375	$C_4H_7NO_4$	11.92	0.019	0.032	4.5	1.00	YES	51.1	1.51	HMDB00191
Creatinine	113.0589	$C_4H_7N_3O$	13.57	0.014	0.027	10.6	1.02	YES	26.4	1.26	HMDB00562
Phenylalanine	165.0789	$C_9H_{11}NO_2$	14.33	0.014	0.027	9.9	1.05	YES	48.3	1.48	HMDB00159
N-acetyl-aspartic acid	175.0481	$C_6H_9NO_5$	14.75	0.011	0.025	10.2	1.05	YES	35.4	1.35	HMDB00812
Allothreonine	119.0582	$C_4H_9NO_3$	16.14	0.0019	0.0078	23.6	1.12	YES	60.9	1.61	HMDB04041
Cholesterol and derivatives											

Cholesterol	386.3549	$C_{27}H_{46}O$	27.61	0.014	0.027	3.8	1.00	YES	22.7	1.23	HMDB00067
Cyclic polyalcohols											
Scyllo-Inositol*	180.0633	$C_6H_{12}O_6$	18.67	0.024	0.038	6.5	1.03	YES	26.6	1.27	HMDB06088
Myo-inositol	180.0633	$C_6H_{12}O_6$	19.29	0.0012	0.0060	8.5	1.20	YES	47.9	1.48	HMDB00211
Dicarboxylic acids and derivatives											
Succinic acid	118.0266	$C_4H_6O_4$	10.44	0.0040	0.0132	3.8	1.07	YES	41.6	1.42	HMDB00254
Fumaric acid	116.0110	$C_4H_4O_4$	10.94	0.0028	0.0096	23.8	1.12	YES	35.6	1.36	HMDB00134
Fatty Acyls											
Caproic acid	116.0837	$C_6H1_2O_2$	7.05	0.011	0.025	6.4	0.99	YES	122.8	2.23	HMDB00535
Hydroxy acids and derivatives											
Lactic acid	90.0316	$C_3H_6O_3$	6.83	$7.8x10^{-4}$	0.0049	3.1	1.19	YES	41.8	1.42	HMDB00190
Keto acids and derivatives											
3-methyl-2-oxobutanoic acid	116.0837	$C_6H1_2O_2$	7.50	$8.2\ x10^{-5}$	0.0010	15.3	1.22	YES	33.5	1.33	HMDB00310
Non-metal oxoanionic compounds											
Phosphoric acid	97.9768	H_3O_4P	9.85	$4.1x10^{-5}$	$6.5x10^{-4}$	27.0	1.31	YES	73.0	1.73	HMDB02142
Organic phosphoric acids and derivatives											
O-Phosphoethanolamine	141.019	$C_2H_8NO_4P$	16.18	0.011	0.025	20.8	1.01	YES	43.2	1.43	HMDB00224
Pyridinecarboxylic acids and derivatives											
1-methyl nicotinamide	137.0709	$C_7H_9N_2O$	12.69	0.024	0.038	6.5	1.01	YES	39.2	1.39	HMDB00699
Nicotinamide	122.048	$C_6H_6N_2O$	12.71	0.024	0.038	2.8	1.05	YES	39.8	1.40	HMDB01406
Pyrimidines and pyrimidine derivatives											
Uracil	112.0273	$C_4H_4N_2O_2$	10.76	0.0019	0.0078	12.4	1.06	YES	46.2	1.46	HMDB00300
Sulfinic acids and derivatives											
Hypotaurine	109.0197	$C_2H_7NO_2S$	14.12	0.0012	0.0060	9.7	1.15	YES	68.4	1.68	HMDB00965
Ureas											
Urea	60.0323	CH_4N_2O	9.42	0.0028	0.0096	4.1	1.15	YES	69.7	1.70	HMDB00294

654

655 Table 2. Metabolites that showed statistical significance after UVDA and MVDA of NVD *vs* WT
656 comparison. Mass (DB), mass found in the Human Metabolome Database (HMDB)
657 (http://www.hmdb.ca/); RT, retention time expressed in minutes; *p* value, obtained after
658 Student's *t* test; *p*BH, corrected *p* value obtained by Benjamini–Hochberg test correction; CV,
659 coefficient of variation of the metabolites in the QC samples; VIP, VIP values higher than 1 were
660 considered as significant; JK, Jackknife confidence interval; FC, fold change in the comparison.
661 *Metabolites identified by NIST library.

COMPOUND NAME	RT (min)	COMPOUND NAME	RT (min)	COMPOUND NAME	RT (min)
1. Ethanolamine 2	6.450	33. Fumaric acid	10.935	65. Dehydroascorbic acid 1	16.846
2. Artifact 1	6.554	34. Serine 2	11.060	66. Tagatose 2	17.090
3. Pyruvic acid	6.669	35. Acetamide	11.060	67. Fructose 1	17.090
4. Lactic acid	6.832	36. Threonine 2	11.398	68. Sorbose 2	17.184
5. Hexanoic acid	7.051	37. Aspartic acid 1	11.923	69. Tyrosine 1	17.297
6. Glycolic acid	7.057	38. 3-aminoisobutyric acid 2	12.380	70. Galactose 1	17.322
7. Alanine 1	7.451	39. Aminomalonic acid	12.499	71. Altrose 1	17.353
8. 3-Methyl-2-oxobutanoic acid 1	7.504	40. Nicotinamide 2	12.712	72. Talose 1	17.353
9. Acetoacetate 1	7.657	41. Malic acid	12.718	73. Glucose	17.415
10. Glycine 2	7.726	42. Aspartic acid 2	13.124	74. Talose 2	17.559
11. Sarcosine	7.989	43. Trans-4-hydroxy-L-proline 2	13.143	75. Allose 2	17.559
12. Leucine 1	8.252	44. Glutamic acid 3 (dehydrated)	13.156	76. Lysine 2	17.641
13. Mimosine 1	8.790	45. 4-Aminobutanoic acid 3	13.269	77. Mannitol	17.778
14. 3-aminoisobutyric acid 1	9.002	46. 4-guanidinobutyric acid 2	13.275	78. Tyrosine 2	17.810
15. Valine 2	9.065	47. Glutamic acid 1	13.287	79. Pentadecanoic acid (IS)	17.900
16. beta-Alanine 3	9.365	48. Threonic acid	13.393	80. Glucopyranose 5	18.154
17. Urea	9.422	49. Creatinine	13.569	81. Mannose 5	18.154
18. Benzoic acid	9.565	50. Hypotaurine	14.119	82. Scyllo-Inositol 6	18.667
19. Serine 1	9.672	51. Glutamic acid 2	14.332	83. Palmitic acid	18.879
20. Ethanolamine 3	9.803	52. Ornithine	14.332	84. Myo-inositol	19.286
21. Phosphoric acid	9.853	53. Phenylalanine 2	14.332	85. Methyl Stearate (IS)	19.661
22. Leucine 2	9.859	54. N-acetyl-aspartic acid 1	14.751	86. Tryptophan 2	20.349
23. Glycerol	9.872	55. Pyrophosphate	14.788	87. Linoleic acid	20.412
24. Isoleucine 2	10.153	56. Lyxose 2	14.970	88. Oleic acid	20.441
25. Threonine 1	10.184	57. Glycerol 1-phosphate	15.921	89. Stearic acid	20.693
26. Proline 2	10.234	58. N-acetyl-L-phenylalanine 1	15.977	90. Arachidonic acid	21.776
27. 4-Aminobutanoic acid 2	10.281	59. Glutamine 3	16.064	91. Arachidic acid	22.370
28. beta-Alanine 2	10.347	60. Allothreonine 1	16.138	92. Inosine	23.373
29. Glycine	10.353	61. O-phosphocolamine	16.177	93. 1-Monopalmitin	23.504
30. Succinic acid	10.441	62. Hypoxanthine	16.434	94. Cholesterol	27.605
31. Artifact 2	10.460	63. Citric acid	16.540		
32. Uracil	10.760	64. Arabitol 5	16.771		

662

663 Table 3. Compounds designated along the TIC of the optic nerve tissue by GC-MS

Pathways	*p FDR*	*Total metabolites' pathway*	*Hits*	*Metabolites*
Pyrimidine Metabolism	0.0014	36	4	β-alanine, Uracil, Glutamine, 3-Aminoisobutanoic acid
Galactose Metabolism	0.0014	25	2	Glycerol, Myoinositol
Pyruvate Metabolism	0.0017	20	2	Lactic acid, Pyruvic acid
Gluconeogenesis	0.0017	27	2	Lactic acid, Pyruvic acid
Citric Acid Cycle	0.0023	23	4	Citric acid, Fumaric acid, Pyruvic acid, Succinic acid
Mitochondrial Electron Transport Chain	0.0047	15	2	Fumaric acid, Succinic acid
Urea Cycle	0.0076	20	8	Fumaric acid, Glutamic acid, Alanine, Aspartic acid, Ornithine, Pyruvic acid, Urea, Glutamine
Arginine and Proline Metabolism	0.0076	26	6	Fumaric acid, Glutamic acid, Proline, Aspartic acid, Ornithine, Urea
Alanine Metabolism	0.0076	6	3	Glutamic acid, Alanine, Pyruvic acid
Glucose-Alanine Cycle	0.0076	12	3	Glutamic acid, Alanine, Pyruvic acid
Glutathione Metabolism	0.0076	10	2	Glycine, Glutamic acid
Cysteine Metabolism	0.0076	8	2	Glutamic acid, Pyruvic acid
Glutamate Metabolism	0.0076	18	4	Gamma-Aminobutyric acid, Glutamic acid, Succinic acid, Glutamine
Ammonia Recycling	0.0076	18	6	Glycine, Glutamic acid, Serine, Aspartic acid, Pyruvic acid, Glutamine
Protein Biosynthesis	0.0076	19	12	Glutamic acid, Tyrosine, Phenylalanine, Alanine, Proline, Threonine, Lysine, Aspartic acid, Glutamine, Leucine, Valine, Tryptophan
Malate-Aspartate Shuttle	0.0076	8	2	Glutamic acid, Aspartic acid
Sphingolipid Metabolism	0.0076	15	2	Serine, O-Phosphoethanolamine
Methionine Metabolism	0.0076	24	2	Glycine, Serine
Glycine, Serine and Threonine Metabolism	0.017	26	5	Serine, Pyruvic acid, Sarcosine, Glycine, Threonine
Aspartate Metabolism	0.017	12	4	β-Alanine, Fumaric acid, Aspartic acid, N-Acetyl-aspartic acid
β-Alanine Metabolism	0.019	13	3	β-Alanine, Aspartic acid, Uracil
Bile Acid Biosynthesis	0.019	49	2	Cholesterol, Glycine

664

665 Table 4. Quantitative enrichment analysis (QEA) of the metabolic pathways significantly
666 enriched in NVD mice model when compared with the WT group. The enriched metabolite sets
667 listed in the table are ordered by their adjusted *p* values (*p* FDR, False Discovery Rate <5%).

FIGURE CAPTIONS

Figure 1. Scheme of the optic nerve sample treatment prior GC-MS analysis. Legend: MeOH with IS – methanol containing 25 ppm of the Internal Standard pentadecanoic acid; QC – quality control samples.

Figure 2. Bar chart with the experimental values of lactic acid (blue bar) and pyruvic acid (yellow bar). Results are the mean of 8 independent values. The error bars represent the standard error of the mean (SEM).

Figure 3. PCA-X score plots for QC and study samples (A) and only study samples (B) (red dots, NVD samples; purple dots, WT samples; green dots, QCs samples) with an explained variance (R^2) of 0.683 and predicted variance (Q^2) of 0.545 in plot A, and R^2 = 0.724 and Q^2 = 0.581 in plot B. Plot C represents the PLS-DA supervised model R^2 = 0.976 and Q^2 = 0.880. Finally, Plot D represents the supervised OPLS-DA model built with a quality of variance explained and predicted variance (R^2 = 0.998, Q^2 = 0.929), and a percentage of samples correctly classified of 97.2% ± 6.8 SD.

Figure 4. TIC of optic nerve profile obtained by GC-EI-Q-MS. The numbers assigned to each peak correspond to the numbers colored in light blue belong to the two IS spiked to the samples.

Figure 5. Metabolic reaction network of metabolites found in optic nerve tissue samples, obtained with MetScape, a plug-in of Cytoscape software.

Figure 6. Metabolic interconnections between glycolysis, citric acid cycle (TCA cycle) and urea cycle coupled to creatine/creatinine metabolism. Metabolites colored in blue were found as statistically significant after GC-MS data treatment.

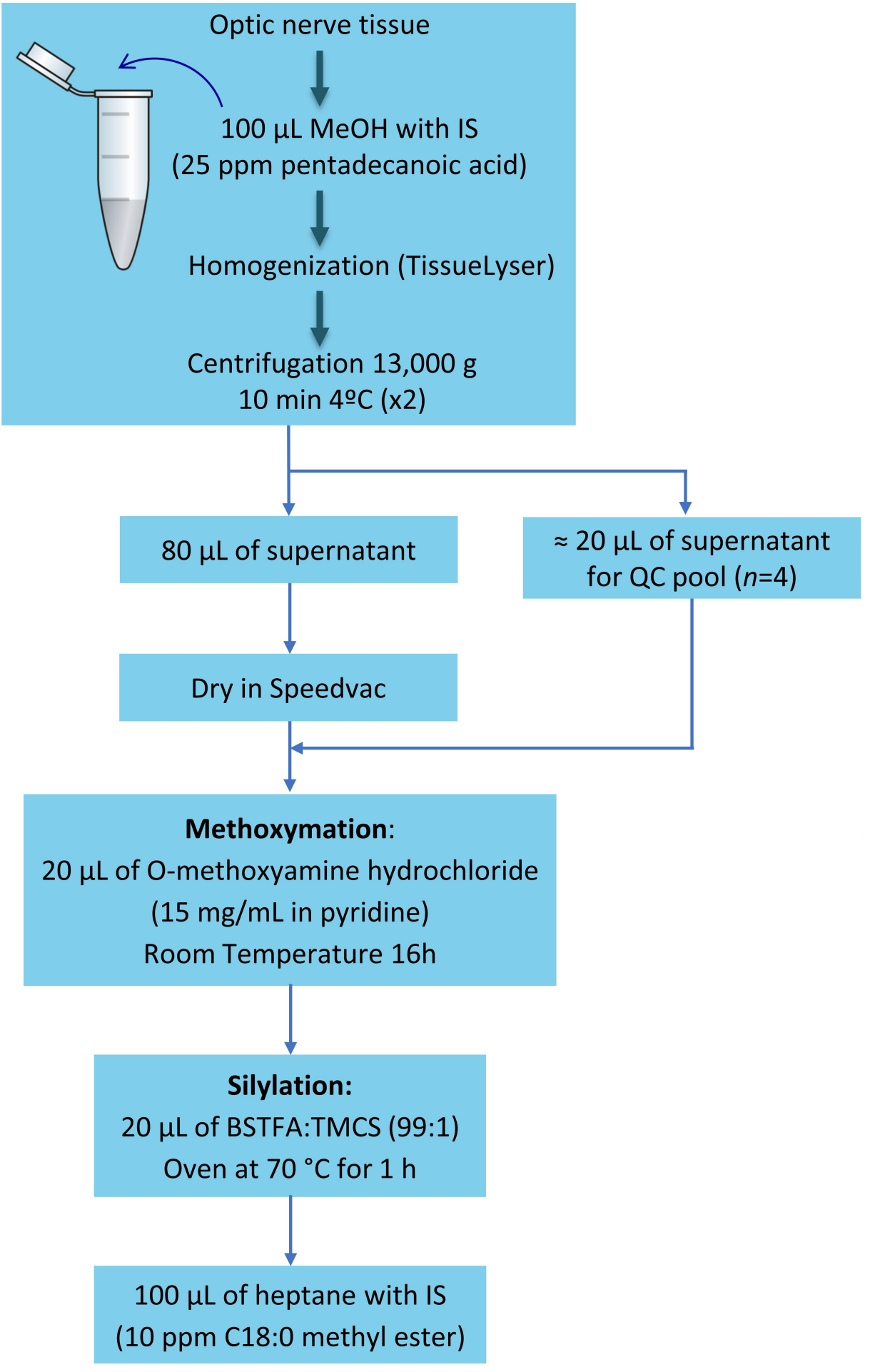
Optic nerve tissue
100 µL MeOH with IS
(25 ppm pentadecanoic acid)
Homogenization (TissueLyser)
Centrifugation 13,000 g
10 min 4ºC (x2)
80 µL of supernatant
≈ 20 µL of supernatant
for QC pool (n=4)
Dry in Speedvac
Methoxymation:
20 µL of O-methoxyamine hydrochloride
(15 mg/mL in pyridine)
Room Temperature 16h
Silylation:
20 µL of BSTFA:TMCS (99:1)
Oven at 70 °C for 1 h
100 µL of heptane with IS
(10 ppm C18:0 methyl ester)

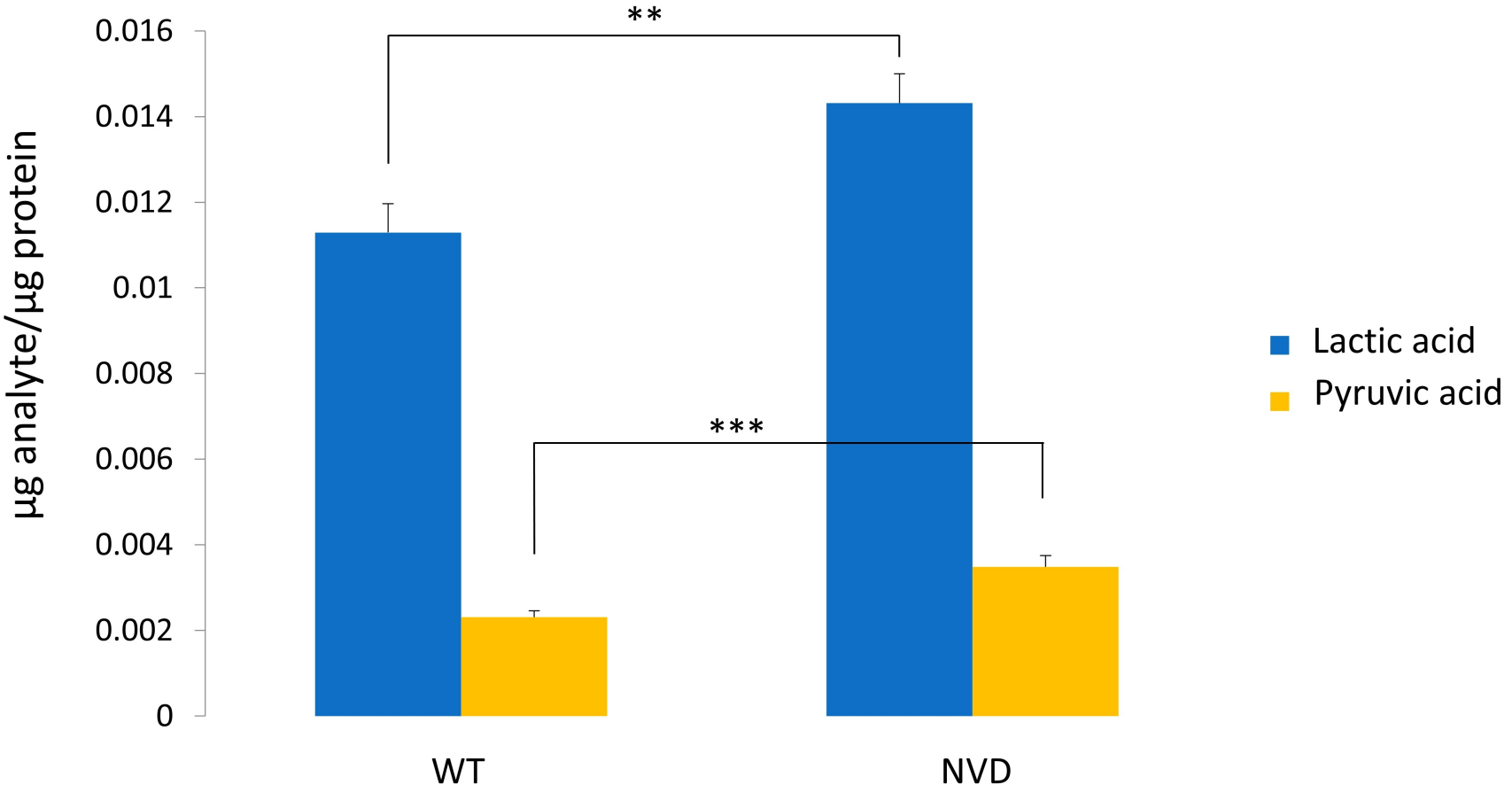
**
***
0.016
0.014
0.012
0.01
0.008
0.006
0.004
0.002
0
µg analyte/µg protein
WT
NVD
Lactic acid
Pyruvic acid

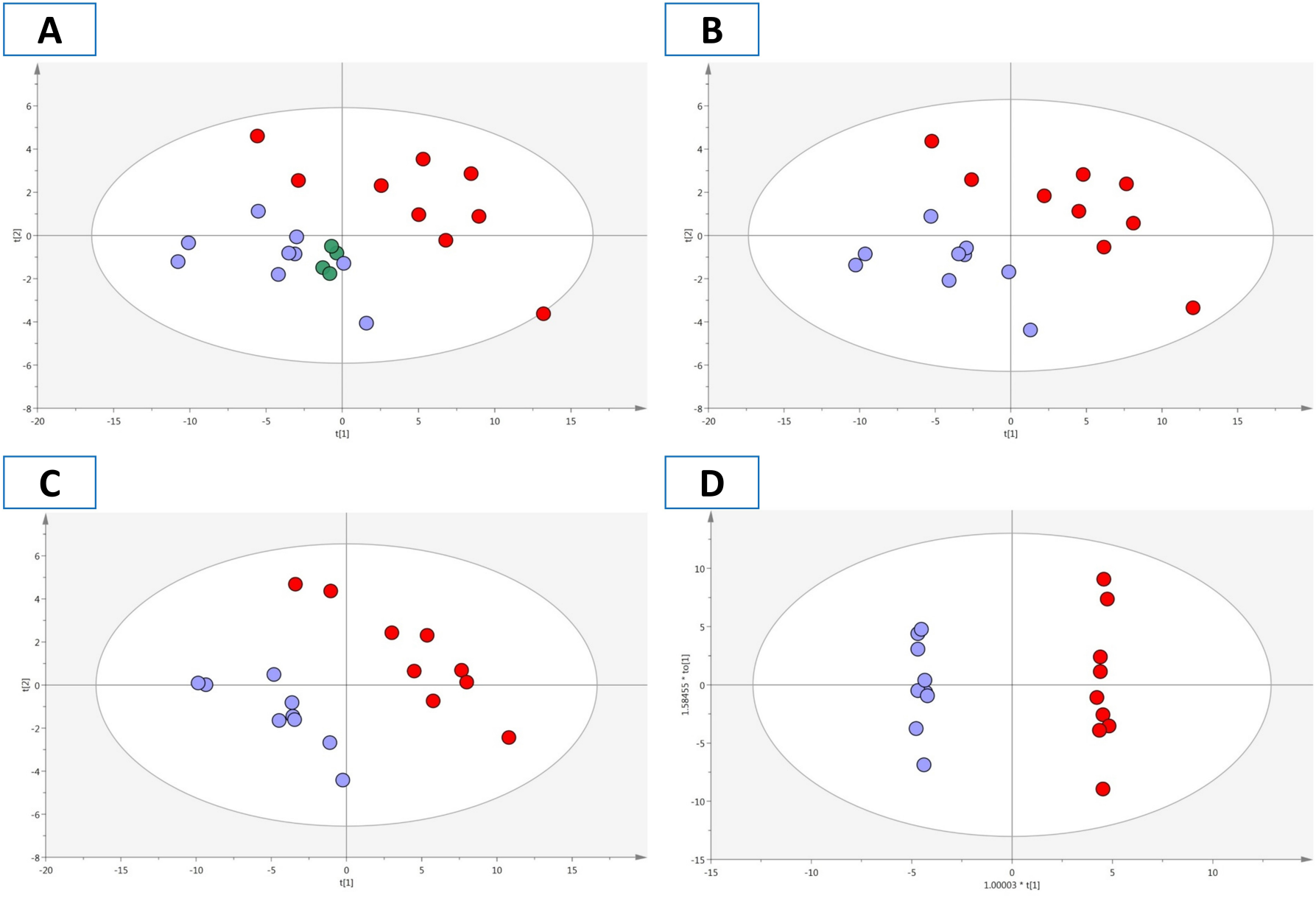
A
B
C
D
t[1]
t[2]
1.58455 * to[1]
1.00003 * t[1]

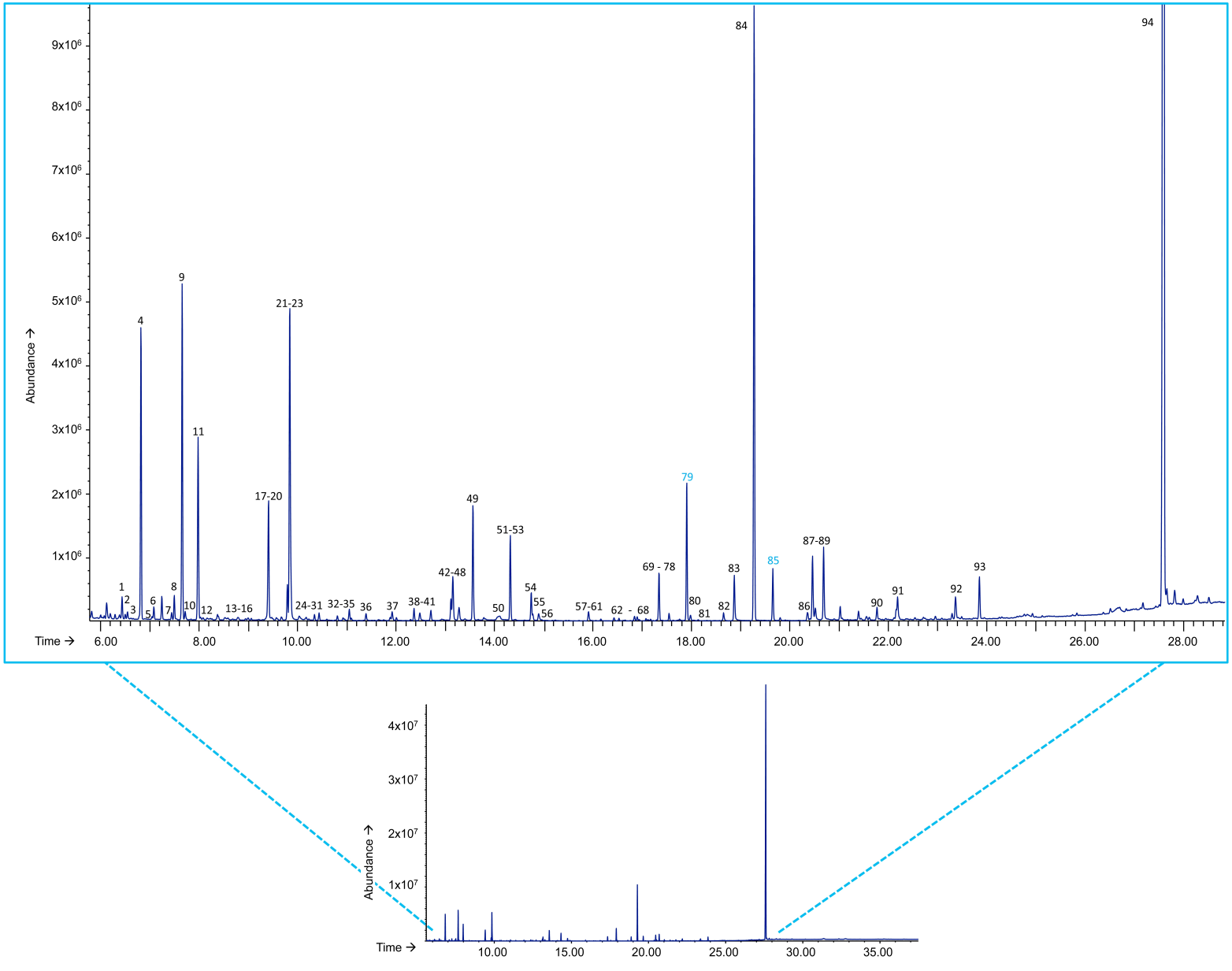
Abundance →
Time →
9x10⁶
8x10⁶
7x10⁶
6x10⁶
5x10⁶
4x10⁶
3x10⁶
2x10⁶
1x10⁶
6.00
8.00
10.00
12.00
14.00
16.00
18.00
20.00
22.00
24.00
26.00
28.00
1
2
3
4
5
6
7
8
9
10
11
12
13-16
17-20
21-23
24-31
32-35
36
37
38-41
42-48
49
50
51-53
54
55
56
57-61
62 - 68
69 - 78
79
80
81
82
83
84
85
86
87-89
90
91
92
93
94
Abundance →
Time →
4x10⁷
3x10⁷
2x10⁷
1x10⁷
10.00
15.00
20.00
25.00
30.00
35.00

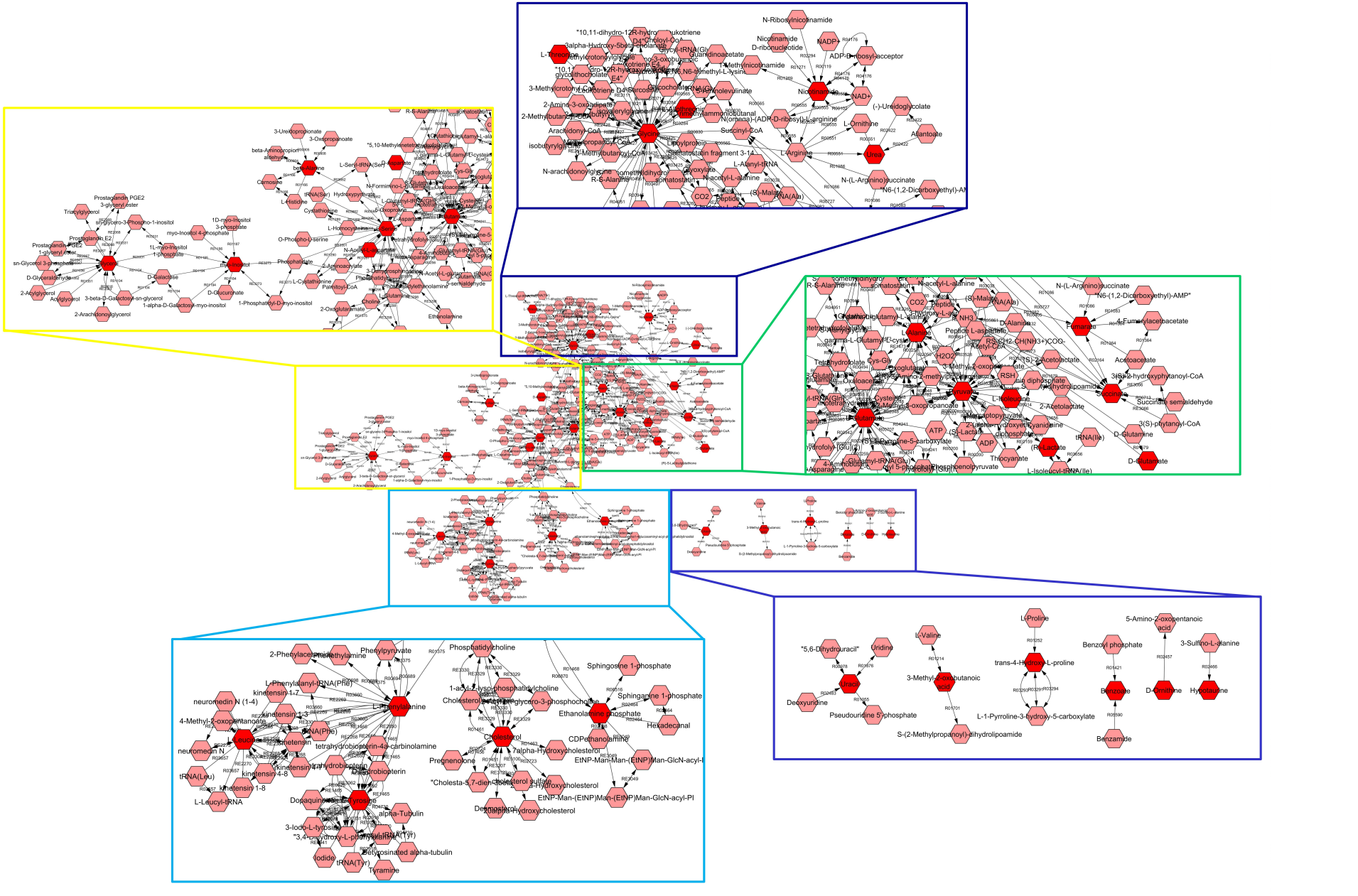
Glycine
Nicotinamide
NADP+
NADH
NAD+
Urea
Glyoxylate
Succinyl-CoA
L-Arginine
L-Ornithine
Allantoate
Fumarate
Acetoacetate
Pyruvate
L-Isoleucine
L-Glutamine
D-Glutamate
Thiocyanate
Ethanolamine
Choline
Phosphatidylcholine
Cholesterol
Sphingosine 1-phosphate
Hexadecenal
Dopaquinone
L-Tyrosine
alpha-Tubulin
Acetylated alpha-tubulin
Tyramine
Uracil
Uridine
Deoxyuridine
Pseudouridine 5'-phosphate
L-Valine
3-Methyl-2-oxobutanoic acid
L-Proline
trans-4-Hydroxy-L-proline
L-1-Pyrroline-3-hydroxy-5-carboxylate
S-(2-Methylpropanoyl)-dihydrolipoamide
Benzoyl phosphate
Benzoate
Benzamide
5-Amino-2-oxopentanoic acid
D-Ornithine
3-Sulfino-L-alanine
Hypotaurine

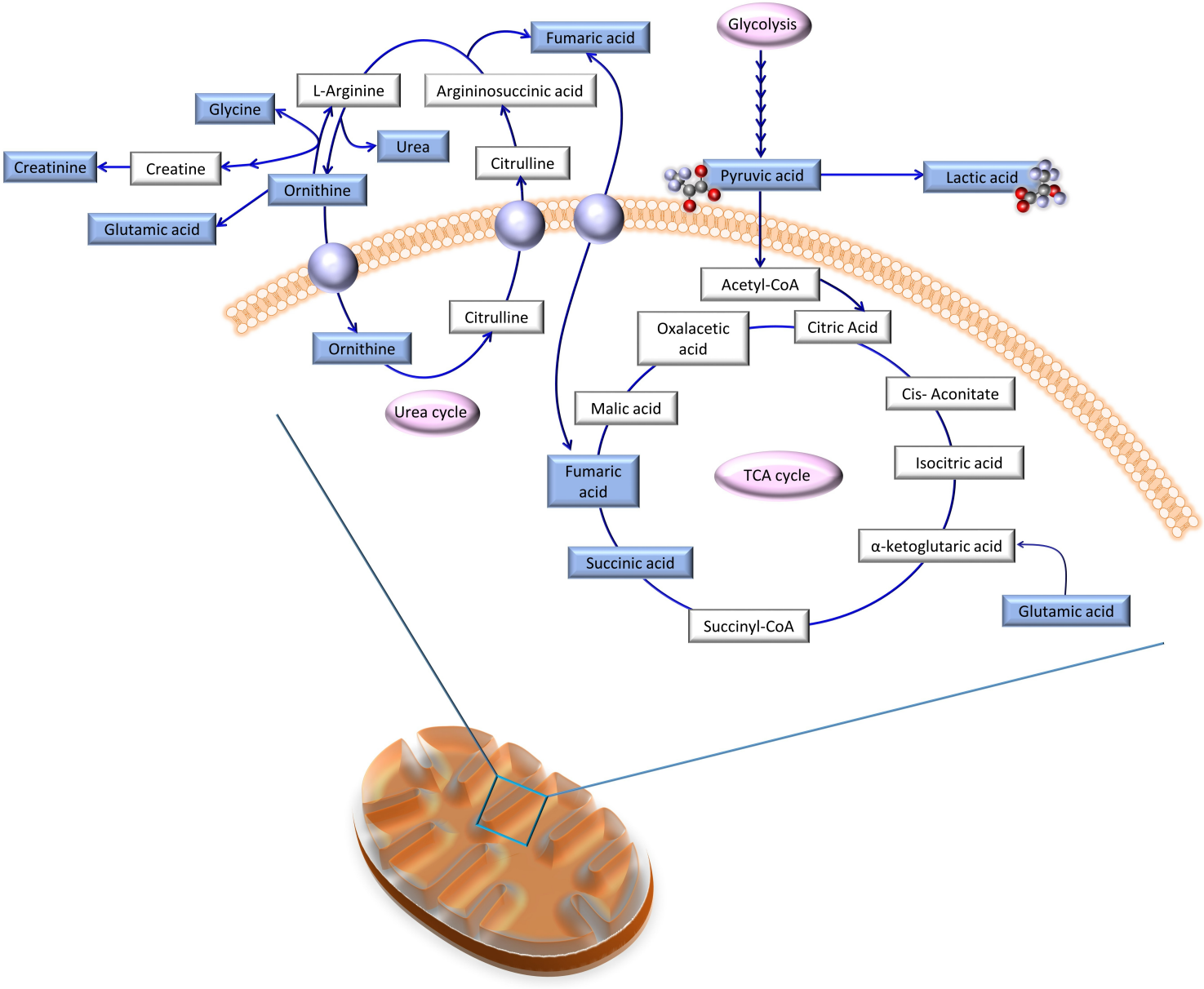
Fumaric acid
Glycolysis
L-Arginine
Argininosuccinic acid
Glycine
Urea
Creatinine
Creatine
Citrulline
Pyruvic acid
Lactic acid
Ornithine
Glutamic acid
Acetyl-CoA
Citrulline
Oxalacetic acid
Citric Acid
Ornithine
Malic acid
Cis- Aconitate
Urea cycle
Fumaric acid
TCA cycle
Isocitric acid
α-ketoglutaric acid
Succinic acid
Glutamic acid
Succinyl-CoA